Secretion of specific metabolites and changes in miRNA expression in murine osteoblastic cells exposed *in vitro* to α-radiation

SATORU MONZEN[1,2], YOTA TATARA[3], MITSURU CHIBA[2,4], YASUSHI MARIYA[5] and ANDRZEJ WOJCIK[6,7]

[1]Department of Radiation Science, Hirosaki University Graduate School of Health Sciences, Hirosaki, Aomori 036-8564, Japan; [2]Research Center for Biomedical Sciences, Hirosaki University Graduate School of Health Sciences, Hirosaki, Aomori 036-8564, Japan; [3]Department of Stress Response Science, Biomedical Research Center, Graduate School of Medicine, Hirosaki University, Hirosaki, Aomori 036-8562, Japan; [4]Department of Bioscience and Laboratory Medicine, Hirosaki University Graduate School of Health Sciences, Hirosaki, Aomori 036-8564, Japan; [5]Cancer for Treatment and Examination Center, Aomori Rosai Hospital, Hachinohe, Aomori 031-8551, Japan; [6]Department of Molecular Biosciences, The Wenner-Gren Institute, Stockholm University, SE-10691 Stockholm, Sweden; [7]Institute of Biology, Jan Kochanowski University, 25-369 Kielce, Poland

Received February 11, 2025; Accepted July 3, 2025

DOI: 10.3892/ijmm.2025.5602

Abstract. Osteoblastic cells (OBCs) in bone marrow (BM) support hematopoietic stem/progenitor cells (HSPCs) by forming a regulatory niche through cytokine and metabolite secretion. Targeted α-emitting radionuclide therapy, such as radium-223 dichloride ($^{223}RaCl_2$), is effective in treating bone metastases but frequently causes unpredictable hematologic toxicities. The underlying mechanism remains unclear. The present study hypothesized that α-radiation alters the OBC secretome and miRNA expression, thereby modulating the BM microenvironment and influencing therapy response. The present study aimed to characterize proteomic, lipidomic and miRNA expression profiles in OBCs following α-radiation exposure. Primary murine BM cells were differentiated into OBCs and irradiated with 0-1 Gy of α-radiation using a ^{241}Am source. Mass spectrometry was used to analyze intracellular proteins and lipids and miRNA expression was assessed by microarray analysis. Kyoto Encyclopedia of Genes and Genomes pathway enrichment was performed using OmicsNet 2.0. α-radiation markedly reduced OBC clonogenic survival and induced specific molecular alterations. A total of six proteins and several lipid species, particularly from the phosphatidylcholine family, showed significant alterations. miRNAs including miR-1895, miR-370-3p and miR-188-5p were downregulated. Enrichment analysis revealed involvement in transcriptional regulation, apoptosis, glycerophospholipid metabolism and cytokine signaling. In conclusion, α-radiation induced distinct proteomic, lipidomic and miRNA changes in OBCs, potentially affecting BM radiosensitivity. These molecules may serve as candidate biomarkers for predicting individual susceptibility to α-emitting radionuclide therapy.

Correspondence to: Dr Satoru Monzen, Department of Radiation Science, Hirosaki University Graduate School of Health Sciences, 66-1 Hon-cho, Hirosaki, Aomori 036-8564, Japan
E-mail: monzens@hirosaki-u.ac.jp

Key words: osteoblast, α-radiation, microRNA, proteomics, lipidomics

Introduction

Osteoblastic cells (OBCs) in bone marrow (BM) produce the bone matrix, participate in bone mineralization and regulate the balance of calcium and phosphate ions in developing bone (1,2). Furthermore, radiosensitive hematopoietic stem/progenitor cells (HSPCs) form a niche with OBCs to maintain the immature state and self-renewal of the BM microenvironment. This tissue is susceptible to the formation of cancerous bone metastases that originate from circulating cells of a primary tumor, represent the terminal stage of cancer and are associated with a reduction in quality of life (3,4). One of the applied treatment modalities is radiation therapy, which is noninvasive. In patients with castration-resistant prostate cancer, bone metastases are curatively treated with radium-223 dichloride ($^{223}RaCl_2$). This therapeutic drug went through a clinical trial called ALSYMPCA and is the world's first internal therapy drug that uses α-radiation. The mechanism of action of this agent is that it accumulates in bone, concentrates on the tumor and has a very large biological effect (5,6).

However, a major problem is that the efficacy and side effects of this therapeutic technique have a high degree of individual variability and patient response is difficult to predict. Hematological adverse events, such as anemia, thrombocytopenia and neutropenia, occur in at least 5% of patients receiving radium-223 therapy (5). The mechanisms underlying the development of these adverse events are unknown; however, α-radiation-induced modulation of OBC activity may be a contributing factor. The self-renewal and differentiation of HSPCs in BM are maintained by cytokines secreted from surrounding cells, including OBCs (7,8). However, unpredictable BM toxicity remains a challenge and it is currently difficult to predict which patients will experience hematologic

adverse effects. As OBCs play a central role in maintaining the BM microenvironment through cytokine and metabolite secretion, The present study hypothesized that α-radiation induced specific molecular alterations in the OBC secretome and regulatory RNAs, which could affect hematopoietic cell behavior or serve as biomarkers of radiation-induced OBC damage. Therefore, the aim of the present study was to characterize the proteomic, lipidomic and miRNA expression profiles of OBCs exposed to α-radiation and to explore the potential of these molecules as indicators of radiosensitivity or predictors of BM toxicity in the context of α-emitting radionuclide therapy.

The present study analyzed the role of OBCs in the regulation of HSPC radiosensitivity. It created an *in vitro* osteoblast metabolic model from mouse primary BM and analyzed the proteins and lipids metabolized by OBCs exposed to α-radiation. Furthermore, The present study focused on the proteomics, lipidomics and transcriptomics of these cells and investigated whether there is a radioresistant component of the hematopoietic system in OBC response to α-radiation.

Materials and methods

Mouse BM cells. The mice study was approved by the Animal Welfare Body in Stockholm University (Djurskyddsorgan; approval number 64-2019) and the Institutional Animal Care and Use Committee in Hirosaki University (approval number AE05-2024-004). All animal experiments were performed in accordance with national animal welfare guidelines and the ARRIVE (Animal Research: Reporting of *In Vivo* Experiments) guidelines (9). Mice were anesthetized using the inhalation anesthetic isoflurane (Pfizer, Inc.). Anesthesia was induced with 4-5% isoflurane and maintained at 2-3% using a small animal anesthesia system. Euthanasia was performed by cervical dislocation under deep anesthesia and death was confirmed by the absence of respiration and heartbeat. Immediately after euthanasia, fresh BM cells were collected from the femurs. C57BL/6N male mice (20-25 g) were delivered at seven weeks of age from a breeding facility, Charles River Laboratories. Upon arrival, the mice were housed under specific pathogen-free conditions with a controlled environment: Room temperature (20˚C), 12-h light/dark cycle and 40-60% relative humidity. At eight weeks of age, mice were anesthetized and euthanized to collect the fresh BM cells. The femurs were excised and cut at both ends using sterile scissors and BM cells were isolated by flushing the marrow cavity with phosphate-buffered saline containing ethylenediaminetetraacetic acid. In total, 30 male C57BL/6N mice were used in the present study. Three groups were based on the α-particle doses: 0 Gy (non-irradiated), 0.5 and 1.0 Gy (n=10 per group). For each mouse, a portion of the collected BM cells was used for the clonogenic cell-forming capacity (CFC) assay and the remaining cells were cultured under osteoblastic differentiation conditions. After differentiation, the cultured cells were used for transcriptomic analysis, while the culture supernatants were analyzed for proteomic and lipidomic profiles.

Differentiation of osteoblastic cells and exposure to α-radiation. The isolated BM cells were seeded in 100-mm round dishes filled with 5 ml of RPMI1640 medium supplemented with 20% fetal bovine serum (Gibco; Thermo Fisher Scientific, Inc.) and incubated for 7 days at 37˚C in a 5% CO_2 atmosphere ($1x10^7$ cells/dish). On day 7, the cells were checked for viability and the differentiation of OBCs was initiated by adding a differentiation medium (20-mM β-glycerol phosphate disodium salt pentahydrate, 100-nM dexamethasone and 50-μM L-ascorbic acid 2-phosphate sesquimagnesium salt hydrate) for 7 days (10). On day 14, cells were exposed to 0.5- or 1-Gy α-radiation (0.22 Gy/min). The radiation exposure was performed on a custom-made dish covered with 2.5 μm thick Mylar foil that allowed the exposure of the cell monolayer to α-radiation from a ^{241}Am source (cat. no. AP1 s/n 101; Eckert and Ziegler) (11). The cells exposed to radiation were incubated for 15 days and the cells were harvested and stored at -80˚C as cell pellets until analysis. For proteomics and lipidomics analyses, a cell pellet was suspended in 7-M urea and 2% sodium dodecyl sulfate and the protein fraction was precipitated by adding acetone. For transcriptomics analyses, total RNAs were extracted using an RNA extraction kit (Qiagen GmbH).

Flow cytometry. The number of BM cells and OBCs expressing the CD45 cell surface antigen was analyzed by flow cytometry system (Moxi GO II; Orflo Technologies) and the results were analyzed by Kaluza software (v.2.2.1; Beckman Coulter Inc.). For this, samples containing $2x10^5$ cells were incubated with the relevant phycoerythrin-cyanin-5-forochrome tandem conjugated anti-mouse CD45 monoclonal antibody (mAb) for 30 min at 4˚C (cat. no. 103109; Biolegend Inc.). Then, erythrocytes including sample cells, were washed using RBC lysis buffer (Thermo Fisher Scientific, Inc.). The intracellular proteins RUNX2 (cat. no. NBP1-77462AF488) and BAP (cat. no. NB110-3638AF488) polyclonal antibody (pAb) (Bio-Techne) were also analyzed using a cell membrane permeation reagent kit (BD Biosciences). Isotype-matched mAb (PE/Cyanine5 Rat IgG2b,κ (cat. no. 400609; Biolegend Inc.) for CD45) or pAb (IgG2a Kappa-FITC (cat. no. 400207; Biolegend Inc.) for BAP and Mouse IgG-FITC (#NBP1-96789, bio-techne Inc.) for RUNX2) was used as negative controls for flow cytometry.

Clonogenic potency assay of hematopoietic BM cells. The clonogenic potency of hematopoietic cells was analyzed using a colony-forming cell (CFC) assay. CFCs, including colony-forming unit-granulocyte and macrophage (CFU-G/GM), burst-forming unit-erythroid (BFU-E) and colony-forming unit-granulocyte, erythroid, macrophage and megakaryocyte (CFU-GEMM), were assayed using the methylcellulose culture kit (MethoCult; Stemcell Technologies, Inc.). The extracted cells from BM or cultured cells were seeded into each well of a 24-well cell culture plate with 300 μl of methylcellulose medium containing recombinant IL-3 (100 ng/ml), recombinant SCF (100 ng/ml), IL-6 (100 ng/ml), G-CSF (10 ng/ml), EPO (4 U/ml), penicillin (100 U/ml; Stemcell Technologies, Inc.) and streptomycin (100 μg/ml) (FUJIFILM Wako Pure Chemical Corporation). The cell culture plate was incubated at 37˚C in a humidified atmosphere containing 5% CO_2/95% air for 7 days. Colonies containing >50 cells were counted under 4x magnification using an inverted microscope (Olympus Corporation). After benzidine staining, the blue and colorless colonies were scored as BFU-E and CFU-G/GM,

Table I. Targeted lipids.

Lipid class	Number of analyses	Analyte abbreviation
Sphingomyeline, Hydroxysphingomyelins	15	SM (OH) C14:1, SM (OH) C16:1, SM (OH) C22:1, SM (OH) C22:2, SM (OH) C24:1, SM C16:0, SM C16:1, SM C18:0, SM C18:1, SM C20:2, SM C22:3, SM C24:0, SM C24:1, SM C26:0, SM C26:1
Diacyl phosphatidylcholine	38	PC aa C24:0, PC aa C26:0, PC aa C28:1, PC aa C30:0, PC aa C30:2, PC aa C32:0, PC aa C32:1, PC aa C32:2, PC aa C32:3, PC aa C34:1, PC aa C34:2, PC aa C34:3, PC aa C34:4, PC aa C36:0, PC aa C36:1, PC aa C36:2, PC aa C36:3, PC aa C36:4, PC aa C36:5, PC aa C36:6, PC aa C38:0, PC aa C38:1, PC aa C38:3, PC aa C38:4, PC aa C38:5, PC aa C38:6, PC aa C40:1, PC aa C40:2, PC aa C40:3, PC aa C40:4, PC aa C40:5, PC aa C40:6, PC aa C42:0, PC aa C42:1, PC aa C42:2, PC aa C42:4, PC aa C42:5, PC aa C42:6
Acyl-alkyl phosphatidylcholine	38	PC ae C30:0, PC ae C30:1, PC ae C30:2, PC ae C32:1, PC ae C32:2, PC ae C34:0, PC ae C34:1, PC ae C34:2, PC ae C34:3, PC ae C36:0, PC ae C36:1, PC ae C36:2, PC ae C36:3, PC ae C36:4, PC ae C36:5, PC ae C38:0, PC ae C38:1, PC ae C38:2, PC ae C38:3, PC ae C38:4, PC ae C38:5, PC ae C38:6, PC ae C40:1, PC ae C40:2, PC ae C40:3, PC ae C40:4, PC ae C40:5, PC ae C40:6, PC ae C42:0, PC ae C42:1, PC ae C42:2, PC ae C42:3, PC ae C42:4, PC ae C42:5, PC ae C44:3, PC ae C44:4, PC ae C44:5, PC ae C44:6
Lysophosphatidylcholine	14	lysoPC a C14:0, lysoPC a C16:0, lysoPC a C16:1, lysoPC a C17:0, lysoPC a C18:0, lysoPC a C18:1, lysoPC a C18:2, lysoPC a C20:3, lysoPC a C20:4, lysoPC a C24:0, lysoPC a C26:0, lysoPC a C26:1, lysoPC a C28:0, lysoPC a C28:1
Total targeted lipids	105	

Cx:y (x, number of carbons in the fatty acid side chain, y,number of double bonds in the fatty acid side chain); OH, hydroxyl; PC, phosphatidylcholine; aa, acyl-acyl; ae, acyl-alkyl; a, lyso; SM, sphingomyelin.

respectively. Statistical analyses were performed using the Origin software package (OriginLab Pro ver. 9.1; OriginLab Corporation). Radiation dose-survival curves were fitted using the algorithm of Levenberg-Marquardt, which combines Gauss-Newton and steepest-descent methods, nonlinear models based on the equation $y=1-[1-\exp(-x/D_0)]^n$, where x indicates the dose in Gy. The values for D_0 (the mean lethal radiation dose) and n (the number of targets) were determined by a single-hit multitarget equation.

Proteomics and lipidomics. The proteins in the harvested cells were precipitated by acetone and lysed with 50% TFE. Reduction and alkylation of proteins were conducted using 10 mM DTT and 20 mM iodoacetamide, respectively. The protein samples were then incubated with trypsin (AB Sciex) overnight at 37˚C. The tryptic peptides were desalted and purified using MonoSpin C18 (GL Sciences). The resulting samples were analyzed using liquid chromatography (LC)-MS/MS with a nanoLC Eksigent 400 system (AB Sciex) coupled with a TripleTOF6600 mass spectrometer (AB Sciex). Peptides were separated using a nano C18 reverse-phase capillary tip column (75 μm x 125 mm, 3 μm; Nikkyo Technos, Co., Ltd.). Peptide separation was performed at 300 nl/min with a 90 min linear gradient of 8-30% acetonitrile in 0.1% formic acid, and then, with a 10 min linear gradient of 30-40% acetonitrile in 0.1% formic acid. Spectra acquired with data-dependent acquisition in positive ion mode were searched using ProteinPilot software (5.0.1; AB Sciex) with the UniProt-reviewed database (https://www.uniprot.org/). The peak areas of individual peptides were extracted using Peakview software (v2.2.0; AB Sciex) with the resulting group files and data-independent acquisition sequential window acquisition of all theoretical fragment-ion spectra (SWATH) spectral data. The peak area values for individual proteins, consisting of the sum of the peak areas of peptides, were normalized to the sum of all proteins detected. Comparisons between sample groups were analyzed using SIMCA software (version 15.0.2; InfoCom Corporation) with multivariate analysis by orthogonal partial least squares discriminant analysis.

Secreted lipids in the culture medium were measured using QTRAP6500+ (AB Sciex) with multiple reaction monitoring methods in the positive ion mode. The transition channels of lysophosphatidylcholine (lysoPC) with acyl residues, acyl-acyl phosphatidylcholine (PC aa), phosphatidylcholine with acyl-alkyl residue sum (PC ae) and sphingomyelin are shown in Table I (10). Lipids were extracted at room temperature using liquid-liquid extraction. The cell-cultured medium was added to 50% methanol and 25% dichloromethane in a glass screw-cap tube. The samples were mixed with internal standards of 15:0-18:1-d7-PC and 18:1-d7 Lyso PC (Merck KGaA). After inverting the tubes 10 times, they were centrifuged at 1,500 x g for 10 min at room temperature. The lower layer was collected and evaporated. The residues were resuspended in methanol containing 0.1% formic acid. The samples were

analyzed in the flow injection analysis using a high-performance liquid chromatography system (ExionLC AD; AB SCIEX). The flow injection analysis (FIA) was done by injecting 20 μl of the sample into the flow of the FIA program, lasting for 5 min and pumping the FIA mobile phase (methanol containing 0.1% formic acid). QTRAP6500+ settings for FIA mode are as follows: Curtain gas, 30; ion spray voltage, 4,500 V; temperature, 300˚C; ion source gas 1, 50 psi; ion source gas 2, 60 psi; CAD gas, 8 psi; entrance potential, 10 V; collision cell exit potential, 15 V. Flow rate settings for FIA are as follows: 0.03 ml/min in 1.6 min; 0.03 to 0.2 ml/min in 0.8 min; 0.2 ml/min in 0.4 min; 0.2 to 0.03 ml/min in 0.2 min. Multiple reaction monitoring (MRM) settings are shown in Table SI. PCs and lysoPCs were normalized to the internal standards. For semi-quantitation of all lipids, the peak areas of individual lipids were normalized to the sum of the peak areas of all lipids detected.

For pathway enrichment analysis, markedly altered proteins and lipid species were subjected to Kyoto Encyclopedia of Genes and Genomes (KEGG)-based annotation and analyzed using OmicsNet 2.0 (https://www.omicsnet.ca/) (12). Functional enrichment analyses were performed to identify affected biological pathways and metabolic processes. The input data consisted of proteins and lipid metabolites that showed statistically significant differences following α-radiation exposure. The six proteins [ITIH3 (Q61704), ATPB (P56480), PDIA3 (P27773), ANT3 (P32261), PDIA6 (Q922R8) and RPL4 (Q9D8E6)] and seven lipid species (PC aa C24:0, PC aa C26:0, PC aa C34:4, PC ae C42:3, PC ae C42:2, PC ae C44:4 and lysoPC a C26:0) selected for KEGG enrichment were identified based on statistically significant fold changes (adjusted $P<0.05$) observed in α-irradiated OBCs compared to controls.

Prior to pathway enrichment and integrated network analyses, all raw proteomics and lipidomics data were deposited in the public database MetaboBank under the accession number MTBKS262 (https://ddbj.nig.ac.jp/public/metabobank/study/MTBKS262/).

Integrated network analysis: To investigate the potential associations among the identified microRNAs, proteomics and lipidomics datasets, The present study performed an integrated network analysis using OmicsNet 2.0. The analysis incorporated markedly downregulated miRNAs (adjusted $P<0.05$) obtained from the microarray results, alongside radiation-responsive proteins and lipids identified in the omics datasets. Protein-protein interaction data were sourced from the STRING database ver. 12 (https://string-db.org/), and miRNA-target relationships were collected from TargetScan ver.8.0 (https://www.targetscan.org/vert_80/) and miRTarBase ver. 9.0 (https://mirtarbase.cuhk.edu.cn/~miRTarBase/miRTarBase_2025/php/index.php). Special attention was given to two microRNA target genes, ELF4 and LARS2, which were selected based on their expression patterns and biological relevance in the transcriptome data. The interaction networks were constructed to identify potential indirect connections between these genes and the proteins detected in the dataset of the present study. Network visualizations were used to highlight subnetworks suggesting functional interactions related to stress response, mitochondrial activity and transcriptional regulation.

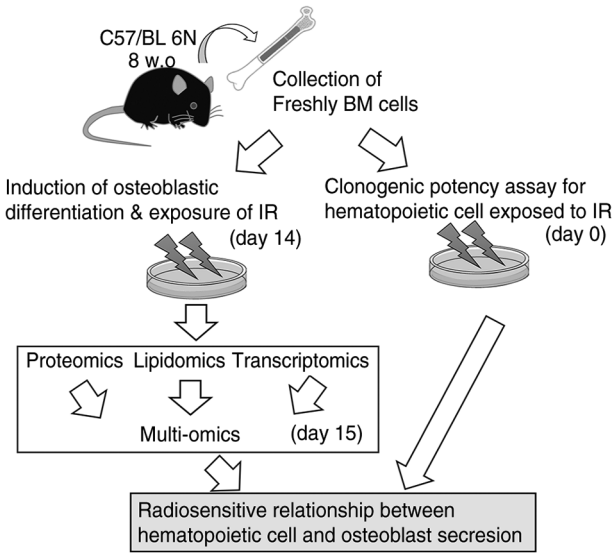

Figure 1. Experimental schematic for preparing OBCs and clonogenic potency assay of hematopoietic cells. BM cells were isolated from the mouse femurs at day 0. Fresh BM cells were plated in a methylcellulose semisolid culture supplemented with an optimal cytokine combination for the clonogenic potency assay. The other cells were cultured and induced to differentiate into osteoblasts on day 7. On day 14, OBCs were irradiated with 0.5-1 Gy. The cell layers and cultured medium were collected on day 15 and prepared for proteomics, lipidomics and transcriptomics analyses. In the present study, a total of 30 mice were used and evenly assigned to three groups (0 Gy, 0.5 Gy and 1 Gy; n=10 mice per group). The BM cells from each mouse were processed independently. A portion of the isolated BM cells was subjected to clonogenic assay, whereas the remaining cells were induced into the osteoblastic lineage for further analyses (transcriptomics, proteomics and lipidomics). OBCs, osteoblastic cells; BM, bone marrow.

MicroRNA microarray analysis: Total RNAs from cultured BM cells were extracted using the RNeasy kit (Qiagen GmbH) according to the manufacturer's instructions. Furthermore, the concentration of total RNAs extracted from cells or tissues was assessed using a NanoDrop spectrophotometer (Thermo Fisher Scientific Inc.). All RNA samples had 260/280-nm absorbance ratios of 1.8-2.0. The quality of small RNAs included in the total RNAs was confirmed by an RNA 6000 Pico kit (Agilent Technologies, Inc.) and a system of Agilent 2100 Bioanalyzer according to the manufacturer's instructions. Cy3-labeled miRNA was synthesized from 30 ng total RNAs using a miRNA Complete Labeling Reagent and Hyb kit (Agilent Technologies, Inc.). A SurePrint G3 miRNA microarray slide (8x60 K, ver. 21.0) for the mouse was hybridized with the Cy3-labeled miRNA in a hybridization solution prepared with a Gene Expression Hybridization Kit (Agilent Technologies, Inc.). Fluorescence signal images of Cy3 on the slide were obtained by a microarray scanner (SureScan; Agilent Technologies, Inc.) and processed by Feature Extraction (version 10.7; Agilent Technologies, Inc.). The raw data of microRNA microarray that was analyzed in the present study was uploaded onto the Gene Expression Omnibus database (GSE286553; https://www.ncbi.nlm.nih.gov/geo/query/acc.cgi?acc=GSE286553).

Statistical analysis: Data are presented as mean ± SD. Statistical analyses were performed using Origin software package (OriginLab Pro ver. 9.1; OriginLab). For comparisons

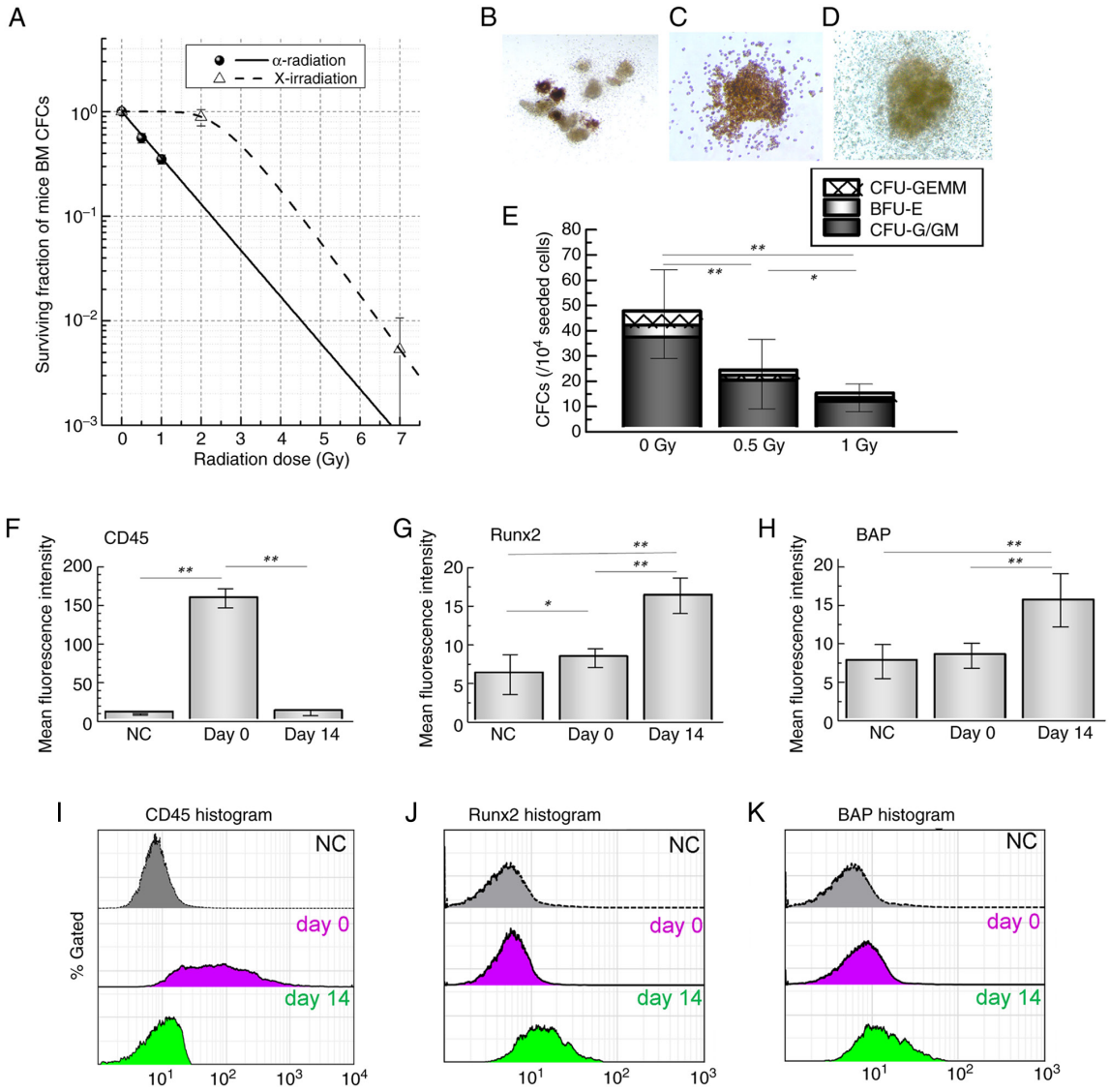

Figure 2. Radiation dose-response of HSPCs and osteoblastic differentiation in mouse BM cells. (A) BM cells were irradiated with α-radiation or X-irradiation and dose-response curves of total CFCs were plotted. Representative images of colony-forming cells (B) CFU-GEMM, (C) BFU-E and (D) CFU-G/GM from BM cultures are shown. (E) Quantification of each colony type is presented. (F-J) Flow cytometric analysis of BM cultures was performed. Quantitative values (F-H) and representative histograms (I-K) are shown for (F and I) CD45 expression and osteoblastic differentiation markers (G and J) RUNX2 and (H and K) BAP. Each value represents the mean ± SD of 8-10 mice per group. Statistical analysis was performed using one-way ANOVA followed by Tukey-Kramer's multiple comparisons test. *P<0.05, **P<0.01 vs. undifferentiated BM-MNCs. HSPCs, hematopoietic stem/progenitor cells; BM, bone marrow; CFCs, colony-forming cells; CFU-GEMM, colony-forming unit-granulocyte, erythroid, macrophage and megakaryocyte; BFU-E, burst-forming unit-erythroid; CFU-G/GM, colony-forming unit-granulocyte and macrophage; MNCs, mononuclear cells ; NC, negative control.

involving more than two groups, one-way analysis of variance was conducted followed by Tukey-Kramer's multiple comparisons test to control for familywise error. All tests were two-tailed unless otherwise specified. P<0.05 was considered to indicate a statistically significant difference.

Results

Clonal growth of BM cells exposed to α-radiation. Freshly isolated BM cells were exposed to 0.5- or 1-Gy α-radiation and plated in methylcellulose-based semisolid culture supplemented with an optimal cytokine combination (Fig. 1). Fig. 2A presents the radiation dose-response curves of hematopoietic progenitors (CFCs). The surviving fractions of CFCs were markedly lower after α-radiation compared with X-irradiation,

Table II. Radiosensitivity of hematopoietic stem/progenitor cells in murine bone marrow.

Radiation type	Radiosensitive parameter	Total CFCs
α-radiation	D_0	0.98±0.42
	n	1.00±0.44
X-radiation	D_0	0.84±0.00
	n	23.01±0.00
RBE	30% survival	2.96±0.23
	10% survival	2.00±0.09

CFCs, colony-forming cells; D_0, mean lethal radiation dose; n, number of targets; RBE, relative biological effectiveness.

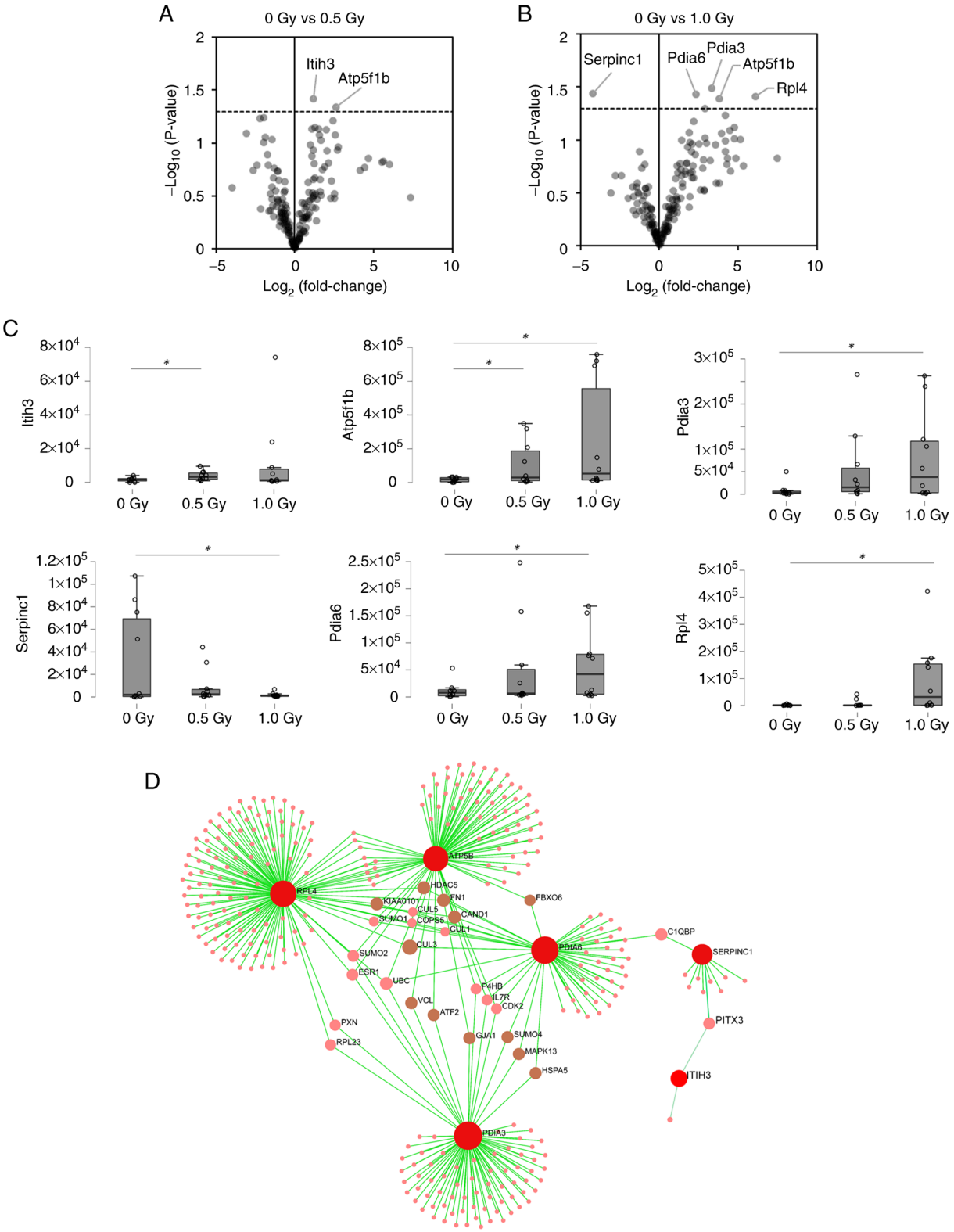

Figure 3. Proteome analysis in irradiated OBCs. Volcano plots comparing (A) 0.5 Gy vs. 0 Gy and (B) 1.0 Gy vs. 0 Gy. Proteins with significant differences (P<0.05; Tukey-Kramer's multiple comparisons test) are labeled. (C) Box plots of the proteins. Groups with significant differences are indicated by asterisks. Rpl4 and Serpinc1 exhibited significant differences in ANOVA among groups (not indicated). The vertical axis represents the relative quantitative values (normalized peak area values) (*P<0.05). (D) Pathway enrichment analysis; markedly altered proteins were subjected to KEGG-based annotation and analyzed using OmicsNet 2.0. Red circles indicate the six key proteins of interest, while pink circles represent predicted proteins that are functionally associated with these six. OBCs, osteoblastic cells; KEGG, Kyoto Encyclopedia of Genes and Genomes.

indicating a higher radiosensitivity. The D_0 and n values are summarized in Table II, confirming this greater sensitivity (D_0: 0.98±0.42 Gy for α-radiation vs. 0.84±0.00 Gy for X-irradiation; n: 1±0.44 vs. 23±0.01, respectively). The relative biological effectiveness (RBE) of α-radiation was calculated to be 2.96 at 30% survival and 2.0 at 10%. Representative images

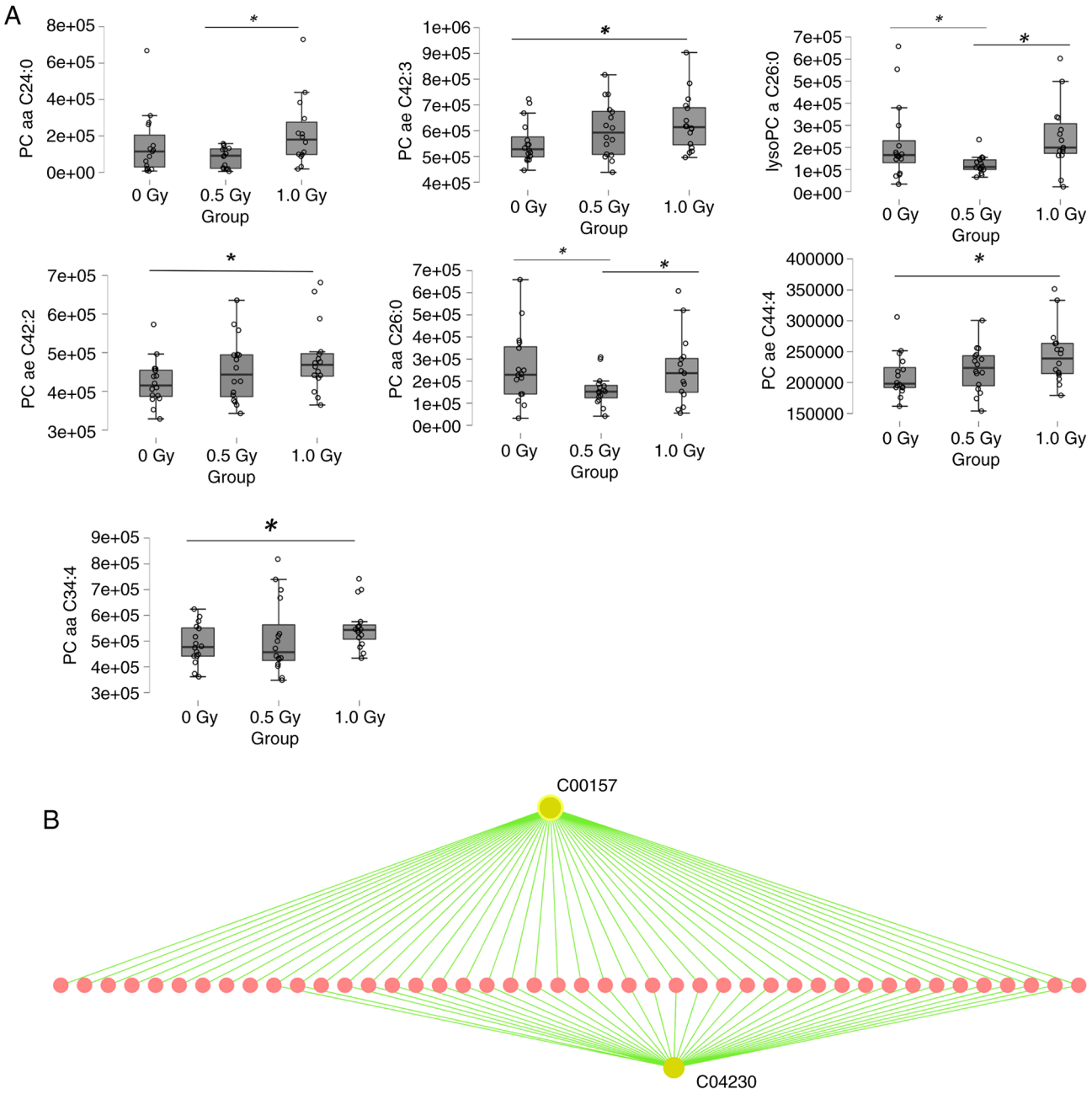

Figure 4. Relative quantities of secreted lipids species in irradiated OBCs. (A) Peak areas of lipids were normalized to the total detected lipid signal. Lipid species showing statistically significant changes compared to non-irradiated controls (*P<0.05, unpaired t-test) are shown. (B) KEGG pathway enrichment analysis based on the markedly altered lipid species using compound IDs (such as C00157 and C04230) was performed to identify associated biological pathways and metabolic processes. OBCs, osteoblastic cells; ; KEGG, Kyoto Encyclopedia of Genes and Genomes.

of CFU-GEMM, BFU-E and CFU-G/GM colonies are shown in Fig. 2B-D, with their quantified colony numbers displayed in Fig. 2E. To assess the effects of radiation on hematopoietic and osteoblastic markers, The present study performed flow cytometry analysis. The corresponding quantitative data are shown in Fig. 2F-H. α-radiation markedly modulated both hematopoietic and osteoblastic differentiation markers in BM-derived cells. Fig. 2I-K shows representative histograms of CD45, RUNX2 and BAP expression, respectively.

Proteomics and lipidomics analysis. The differentiation of BM stromal cells into OBCs was confirmed by the osteoblastic differentiation markers CD45, RUNX2 and BAP (Fig. 2F-K). Proteins extracted from OBCs were measured in the data-dependent acquisition mode and 171 proteins were identified with 95% confidence, satisfying the criteria for SWATH measurement. Of these, two and five proteins were markedly changed in OBCs exposed to 0.5 and 1 Gy of α-radiation, respectively, compared to nonirradiated controls (Fig. 3). The proteins 'protein disulfide-isomerase A3', 'antithrombin-III', 'protein disulfide-isomerase A6', '60S ribosomal protein L4', 'ATP synthase subunit β, mitochondrial', and 'inter-α-trypsin inhibitor heavy chain H3' were detected as specific responses to α-radiation. In the lipidomic analysis, several phosphatidylcholine (PC) and lysophosphatidylcholine (lysoPC) species were markedly changed

Table III. Functional of predictive targeted genes from 24 miRNAs by Gene Ontology (Biological process).

Function name	Number of predictive genes	P-value
Negative regulation of metabolic process	12	0.0455
Endothelial cell proliferation	10	0.038
Macromolecule catabolic process	6	0.0337
Cytokinesis	6	0.0337
Regulation of protein metabolic process	5	0.0369
Sexual reproduction	5	0.042
RNA catabolic process	5	0.0425
Regulation of translation	4	0.00728
Negative regulation of growth	3	0.0314
Translation	3	0.0418
Positive regulation of translation	2	0.0111
RNA 3'-end processing	2	0.0153
Regulation of endothelial cell proliferation	2	0.0309
Regulation of Rho GTPase activity	2	0.0336
Pattern specification process	2	0.0364
Cell projection assembly	2	0.0385
Regulation of signal transduction	2	0.0445

following α-radiation (Fig. 4A). These specific proteins and lipids, showing consistent and statistically significant alterations across biological replicates in response to 0.5 or 1.0 Gy α-radiation, were selected to ensure robust input for pathway enrichment. KEGG pathway enrichment analysis using OmicsNet revealed that the differentially expressed proteins were involved in pathways such as Basal transcription factors, Apoptosis-multiple species and MicroRNAs in cancer (Fig. 3D; Table SII). Similarly, enrichment analysis of the altered lipid species predicted associations with pathways including Glycerophospholipid metabolism, EGFR tyrosine kinase inhibitor resistance, Ether lipid metabolism and Cytokine-cytokine receptor interaction (Fig. 4B, Table SIII).

miRNA expression. RNA microarray analysis of OBCs exposed to α-radiation revealed that 24 miRNAs were markedly downregulated. The data has been deposited in the Gene Expression Omnibus (GEO: GSE286553). The following miRNAs were identified: miR-1894-3p, miR-1895, miR-3072-5p, miR-370-3p, miR-5107-5p, miR-652-5p, miR-6984-5p, miR-7011-5p, miR-7040-5p, miR-7226-5p, miR-8094, miR-8102, miR-188-5p, miR-3081-5p, miR-3098-5p, miR-6538, miR-6969-5p, miR-7020-5p, miR-7044-5p, miR-7048-5p, miR-7082-5p, miR-712-5p, miR-721 and miR-8101. The functions of the genes targeted by these miRNAs were identified using the database OmicsNet 2.0 and included 'negative regulation of metabolic process, endothelial cell proliferation' and 'regulation of protein metabolic process' (Table III). Furthermore, the cellular components 'organelle membrane' and 'Golgi membrane' were identified as targets of these miRNAs (Table SIV). Most target genes were regulated by miR-1895, miR-370-3p, miR-188-5p and miR-712-5p (Fig. 5).

Integrated network analysis of multi-omics data. To investigate potential mechanistic links between the miRNA, proteomics and lipidomics datasets, an integrated network analysis was performed using OmicsNet 2.0. Two representative miRNA target genes, ELF4 and LARS2, were selected based on their biological relevance and expression changes following α-radiation. Although these genes were not directly identified in the proteomic dataset, the analysis revealed that ELF4 was indirectly connected to radiation-responsive proteins such as RPL4, PDIA3, ATP5B and PDIA6 through interaction networks. Similarly, LARS2 was associated with a subnetwork including ATP5B and SERPINC1 (ANT3). These findings suggested indirect regulatory relationships linking α-radiation-induced protein expression changes to downstream gene regulation via miRNA targets. The resulting interaction networks are visualized in Fig. 6, showing the predicted interconnectivity between altered proteins and target genes of radiation-responsive miRNAs.

Discussion

The present study investigated how α-radiation alters the molecular phenotype of BM-derived OBCs, focusing on secreted metabolites and regulatory RNAs. As OBCs play a key role in maintaining the hematopoietic niche through cytokine and metabolite secretion, their radiation-induced dysfunction may influence HSPC radiosensitivity and contribute to BM toxicity observed during α-emitting radionuclide therapies such as ^{223}Ra. To test this hypothesis, the present study applied an integrated omics approach combining proteomic, lipidomic and transcriptomic analyses in murine OBCs irradiated *in vitro*. This multi-layered dataset enabled the examination not only of the direct biochemical effects of α-radiation on OBCs, but also potential signaling pathways involved in hematopoietic dysregulation. It is well established that HSPCs are highly radiosensitive and that cytokine-mediated signaling can modulate this sensitivity (13-15). A-radiation, characterized as high linear energy transfer (LET) radiation, exerts greater biological damage per unit dose than low-LET radiation such as X-rays (16). The findings of the present study were consistent with this notion.

Internal radioactive nuclide therapy using ^{223}Ra, an α-emitting nuclide, markedly enhanced the level of BM toxicity, particularly neutropenia and thrombocytopenia. It is not possible to predict which patients are at increased risk of toxicities (17,18). The self-renewal and differentiation of HSPCs in BM are maintained by various cytokines secreted from surrounding cells, including OBCs (7,8). As OBCs secrete numerous growth factors, differentiation factors and other regulatory cytokines, their secretome may affect the BM response to α-radiation.

The present study accurately quantified the metabolites secreted by OBCs exposed to α-radiation. The concentrations

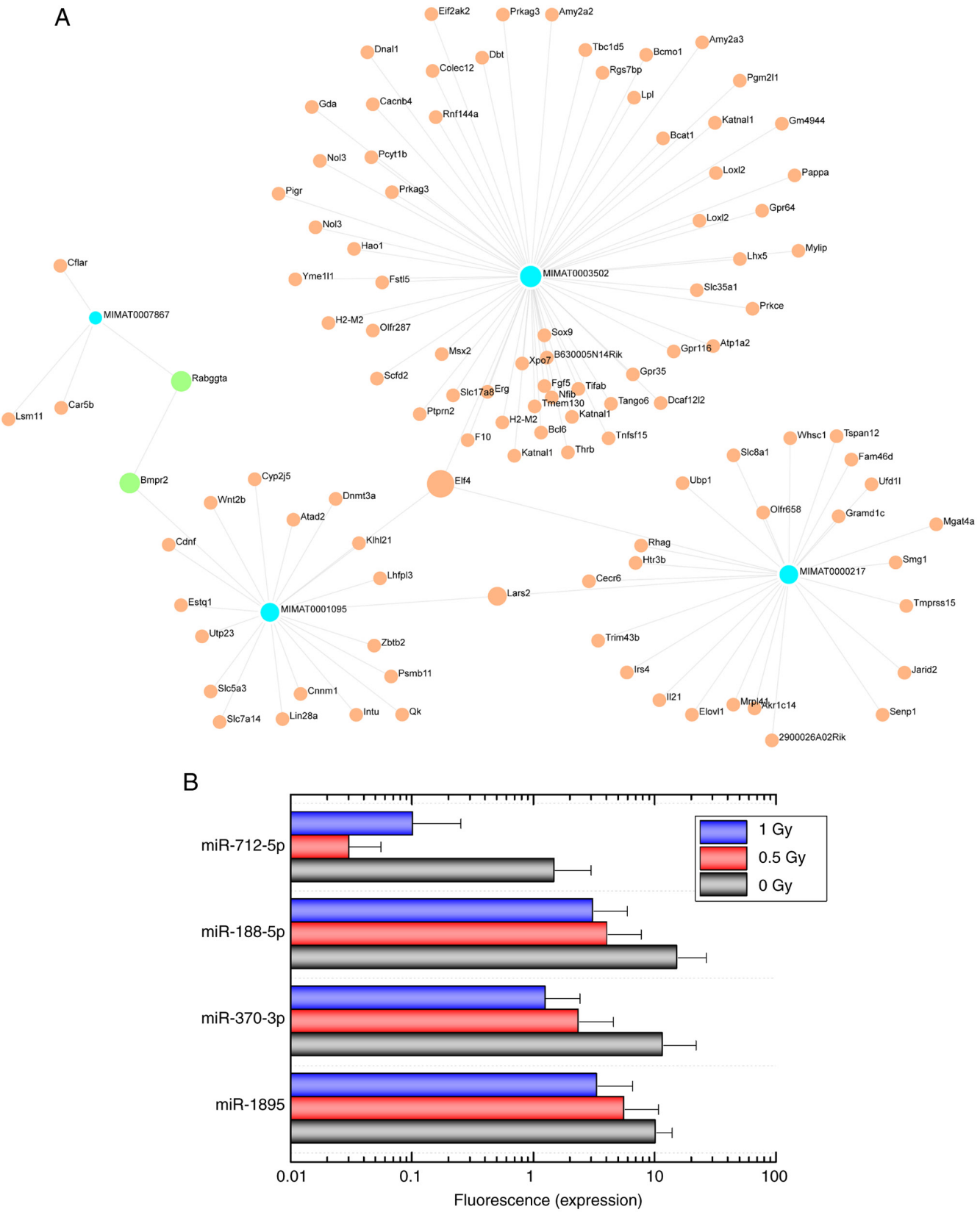

Figure 5. miRNA expression and prediction analysis. (A) The predicted mRNAs (orange color) from the microRNAs (blue color) are shown as a map. The green color shows the predictive proteins. (B) The expression of four focused miRNAs is shown as a bar chart under the 0.5- and 1-Gy dose conditions. The values are presented as mean±SD of separate experiments. miRNA, microRNA.

of five proteins [protein disulfide-isomerase A3 (P27773), protein disulfide-isomerase A6 (Q922R8), 60S ribosomal protein L4 (Q9D8E6), inter-α-trypsin inhibitor heavy chain H3 (Q61704) and ATP synthase subunit beta, mitochondrial (P56480)] were markedly upregulated following exposure to α-radiation compared with the nonirradiated control. By

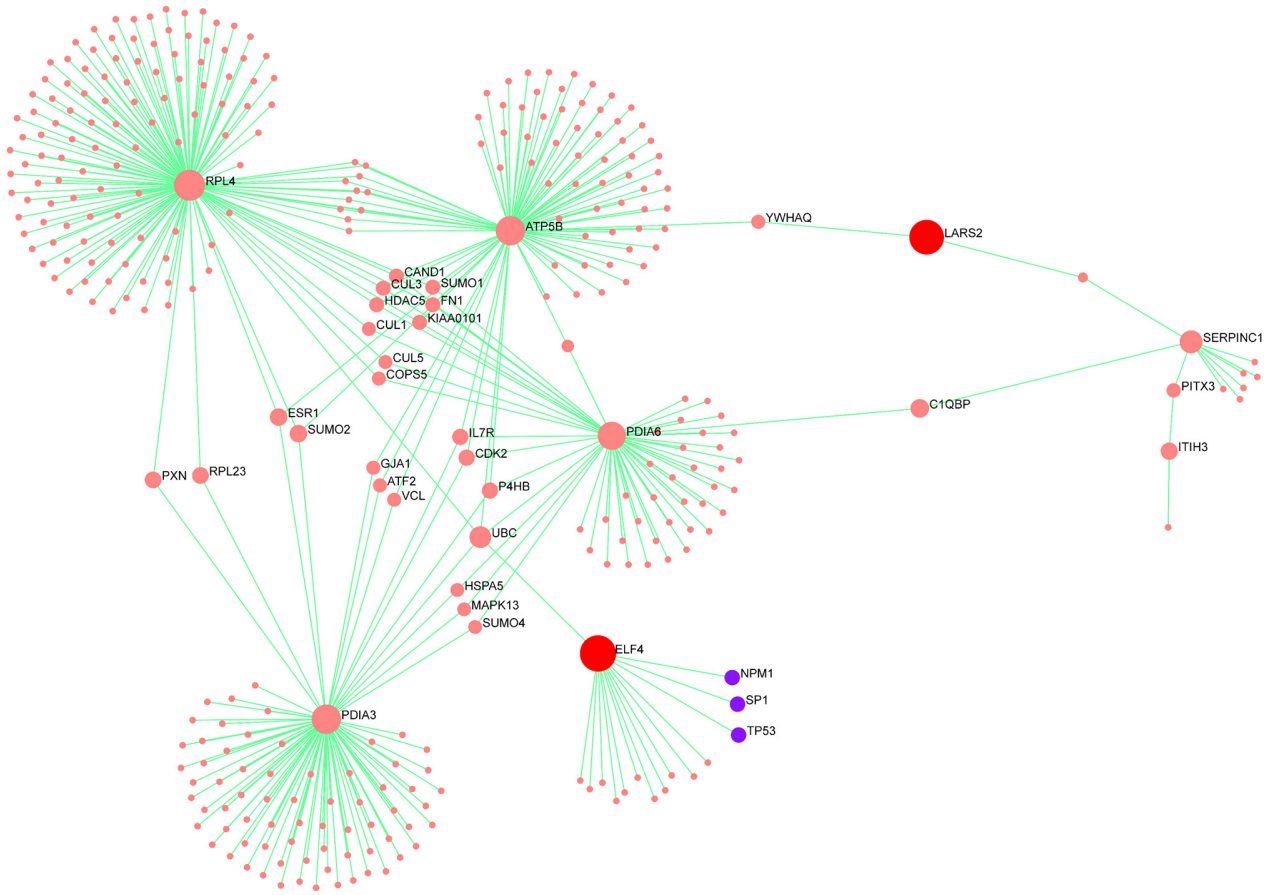

Figure 6. Integrated network of α radiation-responsive proteins and miRNA target genes. The network was generated using OmicsNet 2.0 to illustrate the predicted associations between markedly altered proteins (pink nodes) and target genes of radiation-responsive miRNAs (red nodes), with particular emphasis on ELF4 and LARS2. Transcription factors associated with ELF4 are shown in purple. ELF4 is indirectly associated with RPL4, PDIA3, ATP5B and PDIA6, whereas LARS2 forms a subnetwork involving ATP5B and SERPINC1.

contrast, antithrombin-III (P32261) levels were markedly decreased. In the lipidomics analysis, the concentrations of four lipids (PC ae C42:3, PC ae C42:2, PC ae C44:4 and PC aa C34:4) exhibited a significant upregulation following exposure to 1-Gy α-radiation compared with the nonirradiated controls.

The reason why the secretion of the aforementioned metabolites is modulated by α-radiation is unclear; however, they may act directly or indirectly on cell surface receptors. Another possibility is that they are released due to cell death caused by radiation stress. The cell membrane is a lipid bilayer structure containing phospholipids rich in PC and lysoPC. When apoptosis is induced, cellular tissues are degraded and membrane lipids are released (19).

Although these metabolites are secreted, the expression of small RNAs also changes. In particular, the expression of miR-1895, miR-370-3p, miR-188-5p and miR-712-5p was markedly downregulated by exposure to α-radiation. miRNAs regulate gene expression by binding to the 3'-untranslated regions of target mRNAs, which modulate protein synthesis by increasing mRNA degradation or inhibiting translation (20).

Based on the obtained results, The present study predicted the expression of related mRNAs using OmicsNet and their functions, inferred from Gene Ontology analysis, included 'negative regulation of the metabolic process', 'endothelial cell proliferation', 'macromolecule catabolic process', 'cytokinesis', and 'regulation of protein metabolic process'. Endothelial cells and BM microvascular cells support BM hematopoiesis (21). Furthermore, changes in gene expression related to cell membranes are expected to be related to the disruption of membrane formation induced by apoptosis.

To explore the interplay among different omics layers, the present study conducted an integrated network analysis using OmicsNet 2.0. Although ELF4 and LARS2 were not directly identified in the proteomic dataset, the network analysis revealed biologically plausible associations between these miRNA target genes and radiation-responsive proteins. Specifically, ELF4 was indirectly linked to RPL4, PDIA3, ATP5B and PDIA6; proteins involved in ribosome biogenesis, endoplasmic reticulum stress response and mitochondrial energy production. LARS2 was associated with a subnetwork involving ATP5B and SERPINC1 (ANT3), suggesting its potential involvement in mitochondrial translation and coagulation-related stress pathways. These indirect associations suggest that the downregulation of miRNAs regulating ELF4 and LARS2 may contribute to radiation-induced cellular responses through downstream proteomic alterations. The integrated network, presented in Fig. 6, underscores the potential cross-talk between transcriptional and post-transcriptional regulation in the α-radiation response. The present systems-level view not only strengthened the mechanistic understanding of OBC damage, but also offered potential molecular targets for evaluating or mitigating radiation-induced bone marrow toxicity.

The enrichment analysis was based on a subset of proteins and lipids that were markedly altered following radiation exposure, chosen for their reproducibility and magnitude of change. This targeted approach enhanced the reliability of functional pathway predictions. Furthermore, KEGG-based enrichment analysis was conducted to explore the functional relevance of radiation-induced changes at the proteomic and lipidomic levels. The six proteins showing altered expression following α-radiation were associated with key pathways such as 'Basal transcription factors', 'Apoptosis-multiple species', and 'MicroRNAs in cancer', implying involvement in transcriptional regulation and cell death processes. Similarly, the altered lipid species were predicted to affect 'Glycerophospholipid metabolism', 'EGFR tyrosine kinase inhibitor resistance', and 'Cytokine-cytokine receptor interaction', all of which are functionally linked to membrane remodeling, inflammatory signaling and cell survival under radiation-induced stress. These enrichment results provided mechanistic insight into how OBCs respond to α-radiation at the molecular level and support their potential utility as biodosimetric markers. Currently, no publicly available omics datasets exist for α-radiation-exposed osteoblastic or stromal cells. Unlike prior studies focusing on hematopoietic cells, the present study uniquely applied integrated multi-omics to bone marrow OBCs exposed to α-radiation, revealing novel molecular signatures that may underlie radiation-induced bone marrow toxicity. Thus, the present study served as a foundational *in vitro* model to identify candidate radiation-responsive markers. Future studies involving clinical samples from patients treated with α-emitting radionuclides (for example, ^{223}Ra) are warranted to validate the translational potential of these findings. Although the present study provided novel insights into the molecular responses of OBCs to α-radiation *in vitro*, further validation using *in vivo* models or clinical BM samples from patients treated with α-emitting radionuclide therapies is necessary to confirm the relevance of these candidate biomarkers in physiological settings. The present study used a limited number of biological replicates (8-10 mice per dose group) due to the technical challenges and resource demands of primary OBC culture and comprehensive multi-omics analyses. While consistent and statistically significant trends were observed, the present study acknowledged that a larger sample size would enhance the robustness and generalizability of these findings. Future studies with increased biological replicates and independent validations are warranted to confirm and extend these results. In addition, although the present study identified radiation-responsive metabolites and miRNAs in OBCs, The present study did not perform functional assays (such as gene knockdown or overexpression) to directly establish causal relationships. Such mechanistic validations were beyond the scope of this initial exploratory study but remain essential future directions to clarify the biological roles of these candidate molecules.

In summary, the results indicate that exposure of OBCs to α-radiation leads to altered secretion of metabolites and changes in the expression of related miRNAs. The metabolites may be OBC damage markers in α-radiation therapy to predict individual therapy responses.

In conclusion, the present study presents a comprehensive multi-omics characterization of osteoblastic bone marrow cells exposed to α-radiation, providing new insights into their molecular responses. While the findings highlight key biological alterations associated with high-LET exposure, several limitations remain. Notably, the present study did not include comparisons with other types of radiation, such as γ or β rays. Although the present study focused on α-radiation due to its clinical relevance in ^{223}Ra-targeted therapy, future work should include comparative analyses with other radiation types (such as X-rays, γ rays, or β radiation) to delineate the specificity of the observed omics responses to high-LET radiation. Such comparisons would provide a more comprehensive understanding of radiation-induced molecular changes across different LET contexts.

Acknowledgements

The authors are grateful to Mrs. Miyu Miyazaki of the Scientific Research Facility Center of Hirosaki University Graduate School of Medicine for the mass spectrometry assistance.

Funding

The present study was supported by JSPS KAKENHI, Grants-in-Aid for Scientific Research (B) (Project No. 21H02861/23K21419, Satoru Monzen) and JSPS KAKENHI, Fund for the Promotion of Joint International Research (Fostering Joint International Research; project no. 17KK0181, Satoru Monzen).

Availability of data and materials

The datasets generated and analyzed during the current study are available as follows. The raw microRNA microarray data have been deposited in the NCBI GEO under accession number GSE286553 (https://www.ncbi.nlm.nih.gov/geo/query/acc.cgi?acc=GSE286553). The raw proteomic and lipidomic data have been deposited in MetaboBank under accession number MTBKS262 (https://ddbj.nig.ac.jp/public/metabobank/study/MTBKS262/). All datasets are publicly available and can be accessed through the respective databases.

Authors' contributions

SM, YM and AW designed the study, drafted the manuscript and actively participated in its revision. SM, MC and YT examined and analyzed the experimental data. SM and AW oversaw the manuscript and provided the final approval of the version submitted and published. SM and AW confirm the authenticity of all the raw data. All authors read and approved the final version of the manuscript.

Ethics approval and consent to participate

Not applicable.

Patient consent for publication

Not applicable.

Competing interests

The authors declare that they have no competing interests.

References

1. Amarasekara DS, Kim S and Rho J: Regulation of osteoblast differentiation by cytokine networks. Int J Mol Sci 22: 2851, 2021.
2. Mizoguchi T and Ono N: The diverse origin of bone-forming osteoblasts. J Bone Miner Res 36: 1432-1447, 2021.
3. Clézardin P, Coleman R, Puppo M, Ottewell P, Bonnelye E, Paycha F, Confavreux CB and Holen I: Bone metastasis: Mechanisms, therapies and biomarkers. Physiol Rev 101: 797-855, 2021.
4. Hofbauer LC, Bozec A, Rauner M, Jakob F, Perner S and Pantel K: Novel approaches to target the microenvironment of bone metastasis. Nat Rev Clin Oncol 18: 488-505, 2021.
5. Parker C, Nilsson S, Heinrich D, Helle SI, O'Sullivan JM, Fosså SD, Chodacki A, Wiechno P, Logue J, Seke M, *et al*: Alpha emitter radium-223 and survival in metastatic prostate cancer. N Engl J Med 369: 213-223, 2013.
6. Hoskin P, Sartor O, O'Sullivan JM, Johannessen DC, Helle SI, Logue J, Bottomley D, Nilsson S, Vogelzang NJ, Fang F, *et al*: Efficacy and safety of radium-223 dichloride in patients with castration-resistant prostate cancer and symptomatic bone metastases, with or without previous docetaxel use: A prespecified subgroup analysis from the randomised, double-blind, phase 3 ALSYMPCA trial. Lancet Oncol 15: 1397-1406, 2014.
7. Wilson A and Trumpp A: Bone-marrow haematopoietic-stem-cell niches. Nat Rev Immunol 6: 93-106, 2006.
8. Morrison SJ and Scadden DT: The bone marrow niche for haematopoietic stem cells. Nature 505: 327-334, 2014.
9. Kilkenny C, Browne WJ, Cuthill IC, Emerson M and Altman DG: Improving bioscience research reporting: The ARRIVE guidelines for reporting animal research. J Pharmacol Pharmacother 1: 94-99, 2010.
10. Tatara Y and Monzen S: Proteomics and secreted lipidomics of mouse-derived bone marrow cells exposed to a lethal level of ionizing radiation. Sci Rep 13: 8802, 2023.
11. Staaf E, Brehwens K, Haghdoost S, Pachnerová-Brabcová K, Czub J, Braziewicz J, Nievaart S and Wojcik A: Characterisation of a setup for mixed beam exposures of cells to 241Am alpha particles and X-rays. Radiat Prot Dosimetry 151: 570-579, 2012.
12. Zhou G, Pang Z, Lu Y, Ewald J and Xia J: OmicsNet 2.0: A web-based platform for multi-omics integration and network visual analytics. Nucleic Acids Res 50: W527-W533, 2022.
13. Hérodin F and Drouet M: Cytokine-based treatment of accidentally irradiated victims and new approaches. Exp Hematol 33: 1071-1080, 2005.
14. Takahashi K, Monzen S, Yoshino H, Abe Y, Eguchi-Kasai K and Kashiwakura I: Effects of a 2-step culture with cytokine combinations on megakaryocytopoiesis and thrombopoiesis from carbon-ion beam-irradiated human hematopoietic stem/progenitor cells. J Radiat Res 49: 417-424, 2008.
15. Patterson AM, Wu T, Chua HL, Sampson CH, Fisher A, Singh P, Guise TA, Feng H, Muldoon J, Wright L, *et al*: Optimizing and profiling prostaglandin E2 as a medical countermeasure for the hematopoietic acute radiation syndrome. Radiat Res 195: 115-127, 2021.
16. Goodhead DT: Mechanisms for the biological effectiveness of high-LET radiations. J Radiat Res 40 (Suppl): S1-S13, 1999.
17. Parlani M, Boccalatte F, Yeaton A, Wang F, Zhang J, Aifantis I and Dondossola E: ^{223}Ra induces transient functional bone marrow toxicity. J Nucl Med 63: 1544-1550, 2022.
18. Heidegger I, Pichler R, Heidenreich A, Horninger W and Pircher A: Radium-223 for metastatic castration-resistant prostate cancer: Results and remaining open issues after the ALSYMPCA trial. Transl Androl Urol 7: S132-S134, 2018.
19. Nagata S: Apoptosis and clearance of apoptotic cells. Annu Rev Immunol 36: 489-517, 2018.
20. Valadi H, Ekström K, Bossios A, Sjöstrand M, Lee JJ and Lötvall JO: Exosome-mediated transfer of mRNAs and microRNAs is a novel mechanism of genetic exchange between cells. Nat Cell Biol 9: 654-659, 2007.
21. Rafii S, Shapiro F, Pettengell R, Ferris B, Nachman RL, Moore MA and Asch AS: Human bone marrow microvascular endothelial cells support long-term proliferation and differentiation of myeloid and megakaryocytic progenitors. Blood 86: 3353-3363, 1995.